shape (rather than Lorentzian) for a freely rotating molecule is not fully understood at this moment. An attractive possibility which is consistent with the crystallographic observation of distinct electron density peaks (ordered atomic positions) would be a restricted (jumping) rotation of the molecule such that each atom spends a considerable amount at or near its equilibrium position ("ratchet motion"). A thorough investigation of the temperature dependence of the ^{13}C NMR lineshape and spin-lattice relaxation time (T_1) to probe the details of molecular motion in $C_{60}\cdot CH_2I_2\cdot C_6H_6$ is planned.

The layered nature of the $C_{60}\cdot CH_2I_2\cdot C_6H_6$ crystals opens the possibility, through replacement of some or all of the benzene or methylene iodide molecules with a suitable cation, to build salts of fulleride anions if charge transfer to the layers can be induced. Such salts should be good two-dimensional electrical conductors, possibly even superconductors.

Acknowledgment. Work at Argonne National Laboratory and North Carolina State University is sponsored by the U.S. Department of Energy, Office of Basic Energy Sciences, Divisions of Materials and Chemical Sciences, under Contract W-31-109-ENG-38 and Grant DE-FG05-86ER45259, respectively. B.M.S., S.S.H., and P.R.M. are student undergraduate research participants, sponsored by the Argonne Division of Educational Programs, from the University of Wisconsin at Stevens Point, WI, and Platteville, WI, and from Willamette University, Salem, OR, respectively. We thank Drs. Aravinda M. Kini and Constantino S. Yannoni for fruitful discussions.

Note added in proof: A further analysis of the low-temperature X-ray diffraction data revealed the presence of a minor fraction (<30%) of the C_{60} molecules in a different orientation than that reported here. We thank Dr. Marilyn M. Olmstead and Mr. Bruce C. Noll, University of California at Davis, for suggesting the reanalysis.

Registry No. $C_{60}\cdot CH_2I_2\cdot C_6H_6$, 143124-00-9.

Supplementary Material Available: Atomic coordinates and thermal parameters for $C_{60}\cdot CH_2I_2\cdot C_6H_6$ at 295 K and at 122 K (6 pages); observed and calculated structure factors (24 pages). Ordering information is given on any current masthead page.

Scanning Tunneling Microscopy of the Organic Conductor $[(\eta\text{-}C_5Me_5)_2Ru(\eta^6,\eta^6\text{-}[2_2](1,4)\text{-cyclophane})][TCNQ]_4$

Shulong Li, Henry S. White, and Michael D. Ward*

Department of Chemical Engineering and Materials Science, University of Minnesota, Amundson Hall, 421 Washington Ave. SE, Minneapolis, Minnesota 55455

Received June 5, 1992

Scanning tunneling microscopy (STM) studies of the (001) and (010) faces, of the molecular semiconductor $[(\eta\text{-}C_5Me_5)_2Ru(\eta^6,\eta^6\text{-}[2_2](1,4)\text{cyclophane})]^{2+}[TCNQ]_4^{2-}$ (1, TCNQ = tetracyanoquinodimethane) are reported. The lattice constants determined from the density of states corrugation of the STM images are a = 13.8 ± 0.3 Å, b = 15.9 ± 0.2 Å, c = 16.6 ± 2 Å, β = 88° ± 2°, γ = 82° ± 2°, in good agreement with the X-ray crystal structure. STM images of both faces reveal local density of states (LDOS) associated with stacking of TCNQ molecules along the [100] direction in two crystallographically unique stacks. The tunneling current contrast conforms to the tetrameric periodicity of the TCNQ stacks observed in the crystal structure. Columnar regions of negligible tunneling current on the *ac* face are attributed to stacks of $(\eta\text{-}C_5Me_5)_2Ru(\eta^6,\eta^6\text{-}[2_2](1,4)\text{cyclophane})^{2+}$ dications. Each TCNQ column exhibits a tunneling current corrugation repeating at intervals of a that is attributed to tunneling into the conduction band of antiferromagnetic $2k_F$ charge density wave (CDW) structure. The CDWs also exhibit corrugation, and antiphase modulation, at $a/2$ with respect to adjacent stacks. This is consistent with appreciable interstack Coulomb interactions and contributions from the magnetic $4k_F$ structure, which based on the tight-binding approximation is equivalent to the canonical description $(TCNQ)_2^-(TCNQ)_2^-$. The STM data are in agreement with magnetic susceptibility and EPR studies, which indicate significant contribution of the $4k_F$ state to the electronic structure of 1. The STM therefore provides characterization of the local electronic structure that is manifested in the bulk electronic properties of 1.

Introduction

Crystalline solids based on molecular components exhibit numerous electronic phenomena, including electrical conductivity, superconductivity, nonlinear optical behavior, and ferromagnetism.[1] The most extensively examined molecular crystals have been the low-dimensional conductors and semiconductors, which generally exhibit anisotropic conductivity along axes containing stacks of open-shell charge-transfer molecules that are responsible for the formation of extended band structure. Most notable among low-dimensional molecular crystals are the organic superconductors[2] and, more recently, ferromagnetic materials based on metallocene salts of polycyanoanions.[3] The observation of conductivity and magnetism in extended solids, particularly numerous charge-transfer salts of tetracyanoquinodimethane (TCNQ),[4] suggests a sig-

* To whom correspondence should be addressed.

(1) (a) Lehn, J.-M. *Angew. Chem., Int. Ed. Engl.* **1988**, *27*, 89. (b) *Molecular Electronic Devices*; Carter, F. L., Ed.; Marcel Dekker, New York, 1982. (c) *Extended Linear Chain Compounds*; Miller, J. S., Ed.; Plenum: New York, 1982-1983; Vols. 1-3. (d) Desiraju, G. *Crystal Engineering*; Elsevier: New York, 1989. (e) Miller, J. S.; Epstein, A. J.; Reiff, W. M. *Science*, **1988**, *240*, 40.

(2) (a) Williams, J. M.; Carneiro, K. *Adv. Inorg. Chem. Radiochem.* **1985**, *29*, 249. (b) Inokuchi, H. *Angew. Chem., Int. Ed. Engl.* **1988**, *27*, 1747-1751. (c) Emge, T. J.; Leung, P. C. W.; Beno, M. A.; Wang, H. H.; Firestone, M. A.; Webb, K. S.; Carlson, K. D.; Williams, J. M.; Venturini, E. L.; Azevedo, L. J.; Schirber, J. E. *Mol. Cryst. Liq. Cryst.* **1986**, *132*, 363. (d) Montgomery, L. K.; Geiser, U., Wang, H. H.; Beno, M. A.; Schultz, A. J.; Kini, A. M.; Carlson, K. D.; Williams, J. M.; Whitworth, J. R. *Synth. Met.* **1988**, *27*, A195.

(3) (a) Miller, J. S.; Epstein, A. J.; Reiff, W. M. *Acc. Chem. Res.* **1988**, *21*, 114. (b) Miller, J. S.; Epstein, A. J.; Reiff, W. M. *Science* **1988**, *240*, 40.

0897-4756/92/2804-1082$03.00/0

nificant role for these salts in materials research. The principle advantage of molecular materials is the ability to rationally control bulk properties through molecular design. Further advances in this area, however, require a thorough understanding of the relationship between molecular structure, supramolecular structure, and electronic properties. There also is a need to understand the role of *surface* topographical and electronic structure in the electrochemical crystal growth process[5] that typically is used for synthesis of these materials in order to control crystal size, morphology, growth orientation, and defect density.

Recently, we reported the design and synthesis of $[(\eta\text{-}C_5Me_5)_2Ru(\eta^6,\eta^6\text{-}[2_2](1,4)\text{cyclophane})]^{2+}[TCNQ]_4^{2-}$ (1), which exhibited semiconducting behavior with a room-temperature conductivity of ca. 1 Ω^{-1} cm^{-1}.[6] Single-crystal X-ray structural analysis revealed stacks of TCNQ molecules parallel to the long axes of linear $(\eta\text{-}C_5Me_5)_2Ru(\eta^6,\eta^6\text{-}[2_2](1,4)\text{cyclophane})^{2+}$ dications. This motif was attributed to structural enforcement provided by electrostatic attraction between the oppositely charged ions. The stoichiometry of 1 indicated an average charge of 0.5– per TCNQ molecule (ρ = 0.5, where ρ = average number of carriers on each TCNQ site), equivalent to a one-quarter-filled band for a metallic state. The structure, however, revealed tetrameric periodicity in *two crystallographic unique TCNQ stacks*, suggesting charge localization in the stacks of $(TCNQ)_4^{2-}$. One of these stacks comprised prominent $TCNQ_4$ tetramers separated by a 3.55-Å spacing, while the other exhibited more uniform interplanar spacing. Tetramerization of this ρ = 0.5 salt is consistent with a $2k_F$ insulating spin Peierls structure ($2k_F = \rho/2a$; a = lattice vector), although the actual transition to this structure could not be observed since it evidently occurs at temperatures greater than room temperature. The driving force for the observed lattice distortion may arise from either a lowering of the electron kinetic energy (band energy) according to a classical Peierls distortion or a lowering of the Coulomb energy by formation of charge density waves (CDWs) as with a Wigner crystal.[7]

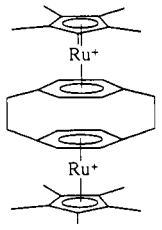

$(\eta\text{-}C_5Me_5)_2Ru(\eta^6,\eta^6\text{-}[2_2](1,4)\text{cyclophane})^{2+}$

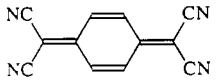

TCNQ

Magnetic susceptibility and electron paramagnetic resonance (EPR) studies of 1[8] indicated the presence of both the antiferromagnetic $2k_F$ spin Peierls ground state and a magnetic insulating $4k_F$ excited state 0.08 eV above the ground state that was manifested in mobile triplet excitons. While the EPR studies indicated a 7.5-Å average separation between the coupled electrons of the triplet, we were not able to elucidate *microscopic* details of the electronic and magnetic behavior such as the contribution of the different TCNQ stacks to the observed behaviors.[9] We therefore were prompted to examine the microscopic electronic structure of 1 with scanning tunneling microscopy (STM).[10]

The tunneling current, i_T, measured in STM is proportional to the density of states (DOS), or $\rho(r,E_F)$, at a position r above the surface and at the Fermi energy, E_F.[11,12] The tunneling current observed on the crystal faces of 1 therefore will depend on the molecular corrugation *and* local density of states (LDOS) of the molecular constituents in the crystal plane. Interpretation of the electronic properties of the highly one-dimensional 1 can be accomplished by use of the tight-binding approximation,[13] in which the states near the Fermi energy comprise linear combinations of the highest occupied molecular orbital (HOMO) or the lowest unoccupied molecular orbital (LUMO) on the constituent molecules. Likewise, it is feasible to interpret STM data, which provide a molecular level view of the electronic structure on a given crystal plane, according to the tight-binding approximation.

Although the tunneling current decays exponentially with distance of the tip from states on the surface of the sample, it is possible that surface regions closer to the tip but with small LDOS will afford minimal tunneling current, and vice versa. Accurate separation of topographical and electronic contributions is especially important when examining molecular crystals which typically are not atomically flat but rather have atoms and portions of molecules protruding from an average surface plane. In this case, the tunneling current will depend on the molecular corrugation *and* LDOS of the molecular constituents in the crystal plane. To develop the capabilities of STM for characterization of molecular crystal surfaces, we have begun to examine crystal planes whose topography can be surmised from known crystal structures. Of particular interest is whether the *surface* electronic structure revealed by STM corresponds to that expected from the known bulk properties. Recently, STM has been used to examine several low-dimensional inorganic conductors[14] and superconductors,[15] as well as organic charge-transfer salts based on bis(ethylenedithiotetrathiafulvalene),[16] tetra-

(4) Broderick, W. E.; Thompson, J. A.; Day, E. P.; Hoffman, B. M. *Science* **1990**, *249*, 401.
(5) Ward, M. D. *Electroanalytical Chemistry*; **1989**, *16*, 181.
(6) Ward, M. D.; Fagan, P. J.; Calabrese, J. C.; Johnson, D. C. *J. Am. Chem. Soc.* **1989**, *111*, 1719.
(7) (a) Torrance, J. B. *Phys. Rev. B* **1978**, *17*, 3099–3103. (b) Torrance, J. B.; Silverman, B. D. *Phys. Rev. B* **1977**, *15*, 788.
(8) Morton, J. R.; Preston, K. F.; Ward, M. D.; Fagan, P. J. *J. Chem. Phys.* **1989**, *90*, 2148–2153.

(9) Pairs of crystallographically unique TCNQ stacks in other charge-transfer salts and their relative contribution to electronic structure, particularly magnetic properties, have been reported; for example: (a) Oostra, S.; Visser, R. J. J.; Sawatzky, G. A.; Schwerdtfeger, C. F. *J. Phys. C* **1983**, *44*, 1381. (b) Schwerdtfeger, C. F.; Wagner, H. J.; Sawatzky, G. A. *Solid State Commun.* **1980**, *35*, 7. (c) Visser, R. J. J.; Smaalen, S. V.; De Boer, J. L.; Vos, A. *Mol. Cryst. Liq. Cryst.* **1985**, *120*, 167. (d) Schwerdtfeger, C. F.; Oostra, S.; Sawatzky, G. A. *Phys. Rev. B* **1982**, *25*, 1786.
(10) (a) Binnig, G.; Rohrer, H.; Gerber, Ch.; Weibel, E.; *Phys. Rev. Lett.* **1982**, *49*, 57. (b) Spong, J. K.; Mizes, H. A.; LaComb, L. J.; Dovek, M. M.; Frommer, J. E.; Foster, J. S. *Nature* **1989**, *338*, 137. (c) Smith, D. P. E.; Horber, H.; Gerber, Ch.; Binnig, G. *Science* **1989**, *245*, 43. (d) Binning, G.; Quate, C. F.; Gerber, Ch. *Phys. Rev. Lett.* **1986**, *56*, 930.
(11) (a) Tersoff, J.; Hamann, D. R. *Phys. Rev. B* **1985**, *31*, 805–813. (b) Tersoff, J. *Phys. Rev. Lett.* **1986**, *57*, 440.
(12) (a) Tekman, E.; Cirai, S. *Phys. Rev. B* **1989**, *40*, 10 286. (b) Tromp, R. M. *J. Phys. Condens. Matter* **1989**, *1*, 10211.
(13) (a) Slater, J. C.; Koster, G. F. *Phys. Rev.* **1954**, *94*, 1498. (b) Bloch, F. *Z. Phys.* **1928**, *52*, 555. (c) Epstein, A. J.; Miller, J. S. *Prog. Inorg. Chem.* **1976**, *20*, 1. (d) Garito, A. F.; Heeger, A. J. *Acc. Chem. Res.* **1974**, *7*, 232–240.
(14) (a) Lieber, C. M.; Wu, X. L. *Acc. Chem. Res.* **1991**, *24*, 170–177. (b) Parkinson, B. A. *J. Amer. Chem. Soc.* **1991**, *113*, 7833–7837.
(15) (a) Wu, X. L.; Lieber, C. M.; Ginley, D. S.; Baughman, R. *J. Appl. Phys. Lett.* **1989**, *55*, 2129. (b) Parks, D. C.; Wang, J.; Clark, N. A.; Hermann, A. M. *Appl. Phys. Lett.* **1991**, *59*, 1506. (c) Coleman, R. V.; Drake, B.; Hansma, P. K.; Slough, G. *Phys. Rev. Lett.* **1985**, *55*, 394–397.

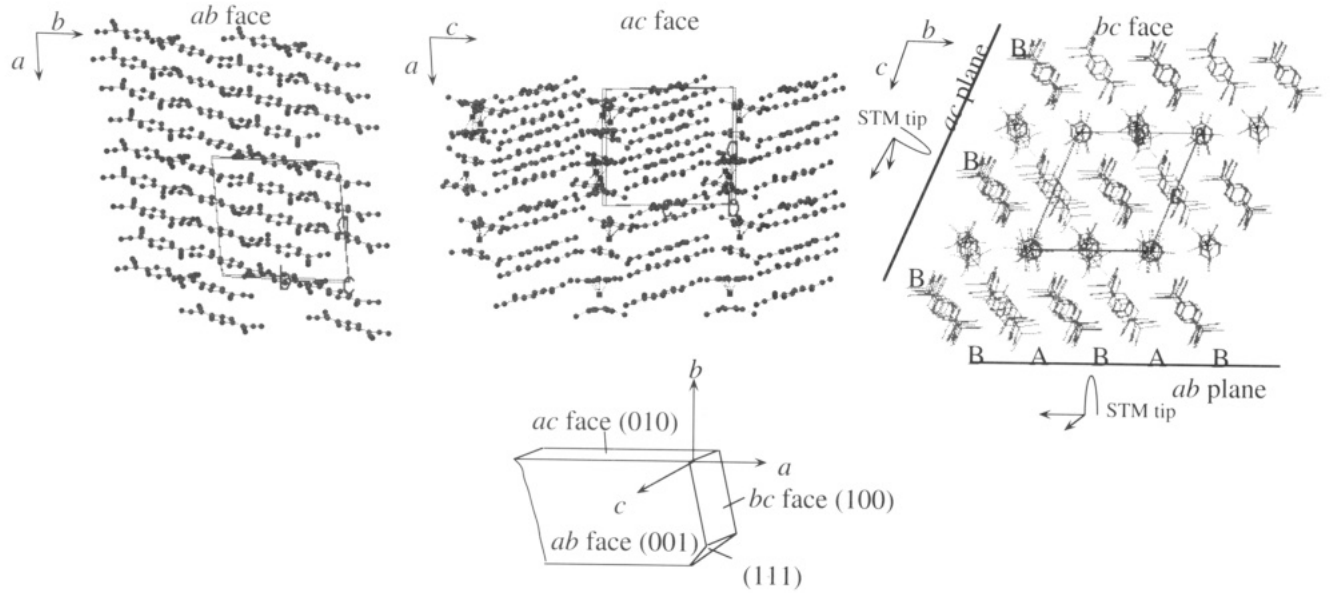

Figure 1. View of 1 normal to the *ab*,*ac*, and the *bc* faces. STM tips on the right panel are drawn as a visual aid to illustrate the scanning direction on the *ac* and *ab* planes, which are normal to the plane of the paper. The *ab* face is depicted here as terminated with both crystallographically unique TCNQ anion stacks, repeating ...ABAB... along the [010] direction. The *ac* face, which has alternating TCNQ anion and $(\eta\text{-}C_5Me_5)_2Ru(\eta^6,\eta^6\text{-}[2_2](1,4)\text{cyclophane})^{2+}$ dication stacks, is depicted with TCNQ stack B (see Figure 2) on the surface plane and stack A in the layer immediately below. The crystal morphology of 1 is depicted with the Miller indices of the faces identified.

Table I. Lattice Constants for $[(\eta\text{-}C_5Me_5)_2Ru(\eta^6,\eta^6\text{-}[2_2](1,4)\text{cyclophane})][TCNQ]_4$ As Determined from X-ray Diffraction and STM[a]

method	*a* (Å)	*b* (Å)	*c* (Å)	α, deg	β, deg	γ, deg
X-ray	13.963	16.107	16.855	67.60	87.30	81.41
STM	13.8 ± 0.3	15.9 ± 0.2	16.6 ± 0.2	*b*	88 ± 2	82 ± 2

[a] Uncertainty in lattice constants determined by STM represents 2σ. [b] α could not be measured since the *ab* face was not investigated.

methyltetraselenafulvalene,[17] tetrathiafulvalenium, and tetracyanoquinodimethane.[18,19] Low-temperature tunneling spectroscopy[20] of organic superconductors, including point-contact studies, to determine the BCS superconducting gap also has been examined with STM.[21] Studies of transition-metal chalcogenides in particular have revealed the capabilities of STM to probe bulk electronic structure.[22]

We describe herein STM investigations of 1 that clearly reveal the presence, on two different crystal faces, of one-dimensional commensurate charge density waves (CDWs) associated with periodic charge localization within the TCNQ stacks. In addition, the contrast of the tunneling current is consistent with contribution from the $4k_F$ structure as well as the $2k_F$ CDW that is evident in the crystal structure. The amplitude of the CDWs of the two crystallographically unique stacks exhibit an anti-phase modulation due to Coulomb correlations between the TCNQ stacks. The results suggest that Coulombic interactions play an important role in the crystal and electronic structure of 1. These studies indicate clearly the value of STM in elucidating the electronic structure of these materials on a molecular level.

Experimental Section

Crystals of 1 were grown by electrochemical reduction of TCNQ (0.20 mmol) on Pt electrodes at 0.30 V (vs SCE) in the presence

(16) (a) Bai, C.; Dai, C.; Zhu, C.; Chen, Z.; Huang, G.; Wu, X.; Zhu, D.; Baldeschwieler, J. D. *J. Vac. Sci. Technol. A* **1990**, *8*, 484–487. (b) Yoshimura, M.; Shigekawa, H.; Nejoh, H.; Saito, G.; Saito, Y.; Kawazu, A. *Phys. Rev. B* **1991**, *43*, 13590–13593. (c) Bando, H.; Kashiwaya, S.; Tokumoto, H.; Anzai, H.; Kinoshita, N.; Kajimura, H. *J. Vac. Sci. Technol.* **1990**, *A8*, 479–483. (d) Yoshimura, M.; Ara, N.; Kageshima, M.; Shiota, R.; Kawazu, A.; Shigekawa, H.; Saito, Y.; Oshima, M.; Mori, H.; Yamochi, H.; Saito, G. *Surf. Sci.* **1991**, *242*, 18–22.

(17) (a) Fainchtein, R.; Murphy, J. C. *J. Vac. Sci. Technol. B* **1991**, *9*, 1013. (b) Pan, S.; Delozanne, A. L.; Fainchtein, R. *J. Vac. Sci. Technol. B* **1991**, *9*, 1017–1021. (c) Li, S.; White, H. S.; Ward, M. D., *J. Phys. Chem.*, in press.

(18) Sleator, T.; Tycko, R. *Phys. Rev. Lett.* **1988**, *60*, 1418.

(19) (a) Magonov, S. N.; Schuchhardt, J.; Kempf, S.; Keller, E.; Cantow, H.-J. *Synth. Met.* **1991**, *40*, 59–72. (b) Magonov, S. N.; Kempf, S.; Rotter, H.; Cantow, H.-J. *Synth. Met.* **1991**, *40*, 73–86.

(20) (a) Blonder, G. E.; Tinkham, M. *Phys. Rev. B* **1983**, *27*, 112. (b) van Bentum, P. J. M.; van Kempen, H.; van de Leemput, L. E. C.; Teunissen, P. A. A. *Phys. Rev. Lett.* **1988**, *60*, 369–372.

(21) (a) Nowack, A.; Weger, M.; Schweitzer, D.; Keller, H. J. *Solid State Commun.* **1986**, *60*, 199–202. (b) Hawley, M. E.; Gray, K. E.; Terris, B. D.; Wang, H. H.; Carlson, K. D.; Williams, J. M. *Phys. Rev. Lett.* **1986**, *57*, 629–632. (c) Maruyama, Y.; Inabe, T.; Yamochi, H.; Saito, G. *Solid State Commun.* **1988**, *67*, 35–37. (d) Nowack, A.; Poppe, U.; Weger, M.; Schweitzer, D.; Schwenk, H. *Z. Phys. B* **1987**, *68*, 41–47. (e) Maruyama, Y.; Hirose, R.; Saito, G.; Inokuchi, H. *Solid State Commun.* **1983**, *47*, 273–274. (f) Bando, H.; Kajimura, K.; Anzai, H.; Ishiguro, T.; Saito, G. *Proc. Seventeenth International Conference on Low-Temperature Physics*, Ecken, U., Schmid, A., Weber, W., Wuhl, H., Eds.; North-Holland: Amsterdam, 1984; pp 713–714. (g) More, C.; Roger, G.; Sorbier, J. P.; Jerome, D.; Ribault, M.; Bechgaard, K. *J. Phys. Lett. (Paris)* **1981**, *42*, L313–L317.

(22) (a) Coleman, R. V.; Giambattista, B.; Hansma, P. K.; Johnson, A.; McNairy, W. W.; Slough, C. G. *Adv. Phys.* **1988**, *37*, 559. (b) Tang, S. L.; Kasowski, R. V.; Parkinson, B. A. *Phys. Rev. B* **1989**, *39*, 9987. (c) Tang, S. L.; Kasowski, R. V.; Suna, A.; Parkinson, B. A. *Surf. Sci.* **1991**, *238*, 280. (d) Wang, C.; Giambattista, B.; Slough, C. G.; Coleman, R. V. *Phys. Rev. B* **1990**, *42*, 8890. (e) Slough, C. G.; McNairy, W. W.; Coleman, R. V.; Garnaes, J.; Prater, C. B.; Hansma, P. K. *Phys. Rev. B* **1990**, *42*, 9255. (f) Dai, Z.; Slough, C. G.; Coleman, R. V. *Phys. Rev. Lett.* **1991**, *66*, 1318. (g) Burk, B.; Thomson, R. E.; Zettl, A.; Clarke, J. *Phys. Rev. Lett.* **1991**, *66*, 1991. (h) Wang, C.; Slough, C. G.; Coleman, R. V. *J. Vac. Sci. Technol. B* **1991**, *9*, 1048. (i) Wu, X. L.; Leiber, C. M. *J. Vac. Sci. Technol. B* **1991**, *9*, 1044. (j) Raina, G.; Sattler, K.; Muller, U.; Venkateswaran, N.; Xhie, J. *J. Vac. Sci. Technol. B* **1991**, *9*, 1039. (k) Slough, C. G.; McNairy, W. W.; Wang, C.; Coleman, R. V. *J. Vac. Sci. Technol. B* **1991**, *9*, 1036. (l) Gammie, G.; Hubacek, J. S.; Skala, S. L.; Tucker, J. R.; Lyding, J. W. *J. Vac. Sci. Technol. B* **1991**, *9*, 1027. (m) Enomoto, H.; Ozaki, H.; Suzuki, M.; Fujii, T.; M. Yamaguchi *J. Vac. Sci. Technol. B* **1991**, *9*, 1022. (n) Giambattista, B.; Slough, C. G.; McNairy, W. W.; Coleman, R. V. *Phys. Rev. B* **1990**, *41*, 10082.

of $(\eta\text{-}C_5Me_5)_2Ru(\eta^6,\eta^6\text{-}[2_2](1,4)cyclophane)^{2+}$ (0.045 mmol) in 0.1 M $n\text{-}Bu_4N^+BF_4^-$/nitromethane as described previously.[6] After several days, large black parallelepiped crystals were obtained on the electrode surface. The crystals exhibited the morphology depicted in Figure 1, with typical crystal dimensions of 4 × 2 × 0.5 mm. The surface areas of crystal faces of **1** decreased in the order (001) > (010) > (100) > (111). All crystals were used as grown, and no additional cleaning or preparation was performed. Crystals were indexed by standard X-ray techniques using an Enraf-Nonius CAD4 computer controlled diffractometer.

A Nanoscope II scanning tunneling microscope with either mechanically cut 80% Pt/20% Ir or 70% Pt/30% Rh tips was used to obtain images. Crystals were mounted with adhesive tape onto an conductive aluminum substrate attached to the STM fixture. Bias voltages ranging from −600 to −1400 mV (tip vs sample) generally could be employed with setpoint currents ranging from 0.10 to 0.30 nA. Images were obtained on the (001) and (010) faces and attempts to examine the (100) face were unsuccessful. Lateral dimensions (x,y) observed in the STM images were calibrated with a graphite standard. Images could be obtained in either constant-current or constant-height mode, but all images shown here were obtained in the constant-height mode owing to the better quality of data obtained. Extended Hückel calculations were performed at the STO-3G level using a Tetronix CACHE molecular modeling workstation.

Results and Discussion

Crystal Structure of 1 and Crystal Plane Topography. Elucidation of the dependence of the tunneling current on the tip distance from LDOS requires understanding of the molecular topography of the crystal plane under examination. The single crystal X-ray structure of **1**, which crystallizes in the $P\bar{1}$ space group (Table I), reveals stacks of dications along the a axis, with adjacent TCNQ stacks nearly parallel to dication stacks (Figure 1). This results in "sheets" of cations and anions in the ab (001) plane that alternate along the [001] direction. Notably, two crystallographically distinct TCNQ stacks are evident, one exhibits a strong tetramerization with a 3.55 Å separation between tetramers (labeled A in Figures 1 and 2). The other (B) exhibits more uniform spacing between TCNQ planes, although a tetrameric repeat motif is still evident. Stack A exhibits a much larger molecular corrugation normal to the stacking a axis as determined from the relative heights of the methylidene carbon atoms normal to the stacking axis (Figure 2, bottom). Assuming a similar density of electronic states on each TCNQ molecule, a larger corrugation of the tunneling current is expected for stack A than for stack B with corrugation length scales equal to that of the tetramer length. If this is indeed the case, these two crystallographically unique stack can be identified in the STM images.

The three principal crystal planes have significantly different molecular topographies. The bc (100) face normal to the stacking axis has rows of dication stacks and TCNQ stacks that alternate along the [001] direction. The (001) face may be terminated with either sheets of cations or anions, although in order to maintain electroneutrality the (001) and (00$\bar{1}$) faces overall must have equal numbers of dications and $[TCNQ]_4^{2-}$ species. The (001) plane is depicted by the solid line at the bottom of the rightmost panel in Figure 1, this plane projecting normal to the plane of the paper. When the (001) face is terminated with anions, it contains *both* crystallographically unique TCNQ stacks alternating ...ABAB... along the [010] direction. The ac (010) plane consists of alternating stacks of dication and TCNQ molecules, but the TCNQ stacks in the surface plane may be either stack A or B. The (010) plane is depicted by the solid line at the left of the right panel in Figure 1, this plane projecting normal to the plane of the paper. In Figure 1, we have depicted arbitrarily this surface plane as containing stack B, with stack A in the next layer.

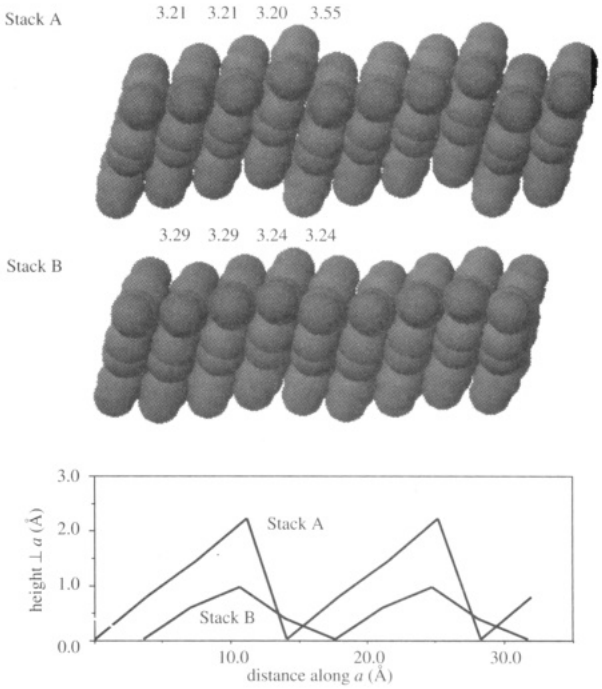

Figure 2. Segments of the two crystallographically independent TCNQ stacks of **1** as viewed along the [010] direction. Stack A is strongly tetramerized with the tetramers separated by 3.55 Å and stack B has more uniform interplanar spacings. The interplanar spacings are indicated above each stack. The line profiles indicate the relative heights along the a axis of the TCNQ methylidene carbon atoms exposed on the ab face.

STM Images. The morphology of crystals of **1** results in large flat faces normal to all three principal directions that are adequate for locating the STM tip on all three principal faces. High-quality images of the (001) and (010) faces were readily acquired. We were not successful, however, in obtaining interpretable images of the (100) face, which is normal to the stacking axis. In addition, high-quality images of the (001) and (010) faces could be obtained only using a negative tip bias (−600 to −1400 mV) and low setpoint currents (0.10–0.30 nA). All attempts to obtain images with a positive tip bias were complicated by an apparent high resistivity which made tip engagement difficult. We attribute this behavior to the semiconducting properties of **1**, as metallic organic conductors are expected to exhibit STM behavior and data that are independent of polarity.

STM images of the (001) face of **1** displayed large, relatively defect-free regions, with molecular flatness over areas exceeding 500 Å × 500 Å (Figure 3). No structures were observed in these regions that might signify transitions between anion and cation covered regions of the (001) plane or monomolecular steps, and images on either side of observed defects were identical. Scans over smaller areas of the (001) face revealed a periodic corrugation of tunneling current along two directions forming an angle of 82° ± 2°, nearly identical to the value of γ determined in the X-ray structure analysis (Figure 4). The tunneling current features repeat along these directions at intervals of 13.8 ± 0.3 and 15.9 ± 0.2 Å, equivalent to the crystallographic unit cell lengths along the a and b axes, respectively (Table I). Notably, two distinct columns with different corrugation patterns are evident, the columns separated by slightly less than $b/2$. We attribute this observation to the known presence of two crystallographically distinct TCNQ stacks. The size of the features in

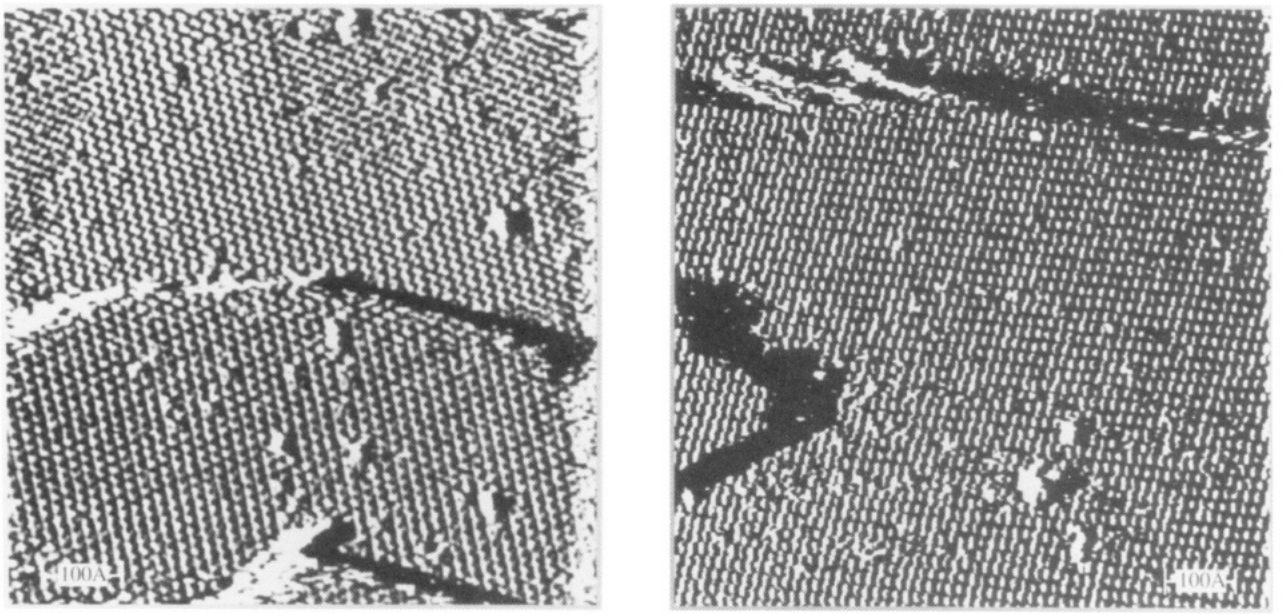

Figure 3. Large-area STM scans of (a) the *ab* (001) face and (b) the *ac* (010) face. Tunneling conditions: tip bias = −651 mV, setpoint current = 0.21 nA. Maximum contrast of tunneling current corresponds to 10 Å. The dimensions of the images are (a) 760 Å × 760 Å and (b) 870 Å × 870 Å.

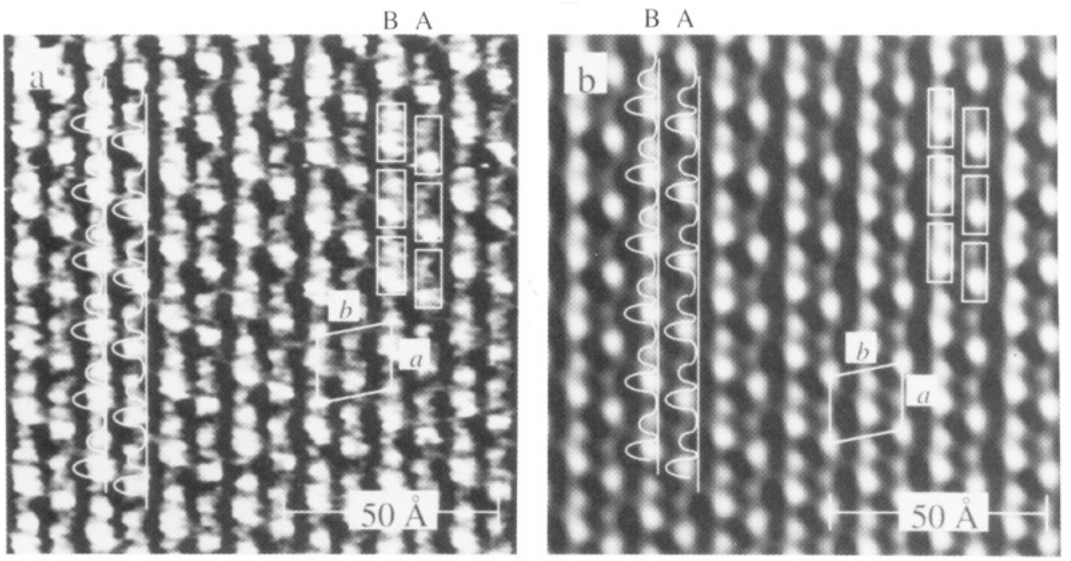

Figure 4. STM images of the *ab* (001) face of **1**: (a) raw data; (b) after Fourier filtering. The rectangular boxes are included as a visual aid to depict the putative tetrameric repeat unit in the two crystallographically independent stacks. The 90° anti-phase modulation between adjacent stacks is illustrated, the amplitude scaling approximately with the tunneling current. Tunneling conditions: tip bias = −651 mV, setpoint current = 0.21 nA. Maximum contrast of tunneling current corresponds to 10 Å.

each column correspond to that expected for the $(TCNQ)_4^{2-}$ tetramers exposed on this face, strongly suggesting that the observed tunneling current reflects a significant localization of state density on these entities (the rectangular boxes in Figure 4 serve as a visual aid for illustrating the tetrameric periodicity). Further examination of the STM image reveals that the tunneling current contrast is significantly larger in one of the columns (column A in Figure 4). This column therefore is assigned to the strongly tetramerized stack A (Figure 2) whose tetramers have greater inclination with respect to the (001) plane (vide supra). This assignment, however, is not definitive as it assumes a uniform density of states within the tetrameric unit. There is no evidence of appreciable LDOS *between* stacks, consistent with a small transfer integral and small bandwidth perpendicular to the stacking direction, factors that favor formation of the $2k_F$ structure.

Closer inspection of the (001) face and analysis of the corresponding line profiles also reveals a secondary corrugation in the DOS contrast in each column at 6.3 Å intervals, corresponding to $a/2$. Fourier-filtered images (Figure 4b) clearly show that the primary features have a "dumbell" shape, suggesting further localization of the DOS within the $(TCNQ)_4^{2-}$ tetramers. The crystal structure of **1** (Figures 1 and 2) does not reveal a *topographical* basis for this observation. That is, there is no severe molecular corrugation at $a/2$ that could account for the diminished tunneling current at $a/2$, suggesting that *modulation of the electron state density* in the TCNQ stacks is responsible for this tunneling behavior. It is also evident that the tunneling current maxima in adjacent columns are out-of-phase with respect to the [010] direc-

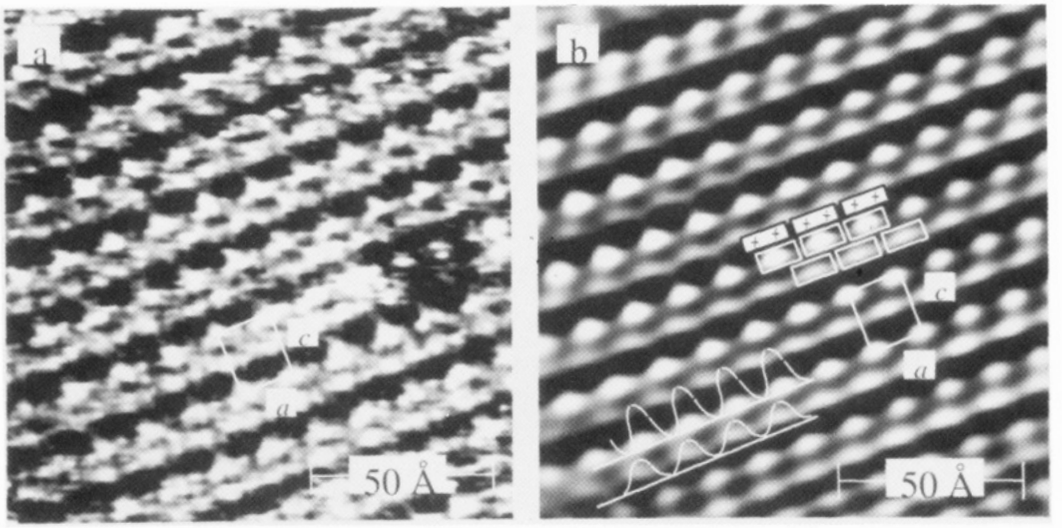

Figure 5. STM images of the *ac* (010) face of **1**: (a) raw data; (b) after Fourier filtering. The rectangular boxes are included as a visual aid to depict the putative tetrameric repeat unit in the two crystallographically independent stacks. The 90° anti-phase modulation between adjacent stacks is illustrated, the amplitude scaling approximately with the tunneling current. Tunneling conditions: tip bias = −1100 mV, setpoint current = 0.09 nA. Maximum contrast of tunneling current corresponds to 20 Å in (a) and 12 Å in (b).

tion as depicted in Figure 4.

STM images of the (010) face (Figure 5) exhibit two columns separated by 6.5 Å with different tunneling current corrugation, with a corrugation repeat distance within each column of 13.8 ± 0.3 Å, in agreement with the lattice parameter a determined from the crystal structure. The magnitude of the tunneling current is similar for the two columns. The periodicity between *pairs* of these columns is 16.6 ± 0.2 Å, equivalent to the c lattice parameter. The angle between these two directions is 88° ± 2°, in good agreement with β determined from the crystal structure. The lattice parameters therefore are consistent with the molecular motif of the (010) plane, which consists of parallel stacks of anions and dications. The tunneling current maxima in adjacent columns are out-of-phase with respect to each other, identical to the behavior observed on the (001) face. The wide region of negligible tunneling current separating the pairs of columns is consistent with the stacks of the insulating closed shell dications which are not likely to have states near E_F. Unlike the (001) face, a corrugation with a length scale of $a/2$ was not evident in STM images of the (010) face.

The good agreement between the periodicity of the tunneling current and the lattice parameters of **1** strongly suggest that the data are attributable to the molecular motif of the (001) and (010) planes obtained directly from the X-ray crystal structure. We do not see any evidence of severe surface reconstruction, nor is it likely that adsorbed impurities can account for the apparently ideal behavior. In addition to occasional steps that separated the large molecular flat regions, line defects were occasionally found in the STM images of the (010) face. The line dislocation in Figure 6 is approximately 10 Å wide and is rather abrupt, clearly showing the interruption of the columns of tunneling current. The nearly identical tunneling current of the average surface plane on each side of the line dislocation suggests that the defect represents a missing row of molecules rather than a step. The direction of the dislocation is roughly along the [401] direction and the mechanism for the formation of the dislocation is not understood at this time.

The observation of two separate columns of tunneling current on the (010) face suggests tunneling into the two crystallographically distinct TCNQ stacks, similar to the behavior observed on the (001) face. This is rather surprising, however, because only one of the crystallographically unique TCNQ stacks is exposed on the (010) surface plane. One of the exocyclic $=C(CN)_2$ groups of each TCNQ molecule in the surface stack protrudes from the surface plane, while the other stack is nestled behind the surface dications. On the basis of the crystal structure, the average separation between the surface stack and the one immediately beneath the surface plane is 7.7 Å, much larger than that suggested by the tunneling current for the two columns. In addition, the *resolved* distance in the (010) plane along the [001] direction between the surface TCNQ stack and the stack immediately beneath the surface plane is only 3 Å, much less than the 6.5 Å separating the columns of tunneling current.[23] While the mechanism

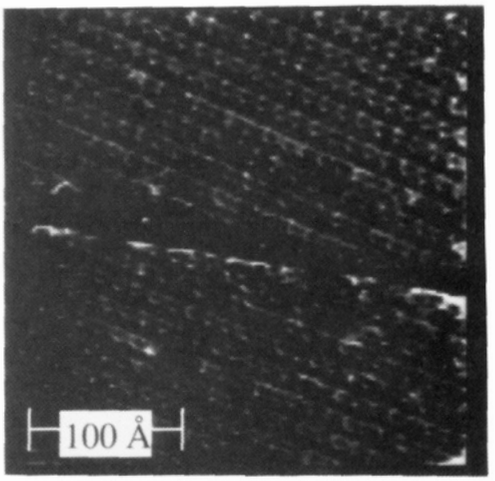

Figure 6. STM image of the *ac* (010) face of **1** depicting a line defect. Tunneling conditions: tip bias = −1100 mV, setpoint current = 0.09 nA. Maximum contrast of tunneling current corresponds to 12 Å.

(23) An alternative explanation for the observation of two columns of tunneling current may involve tunneling into opposite ends of the TCNQ stack on the surface. In this case the *resolved* distance in the (010) plane along the [001] direction between the two ends of the molecule, chosen as the exocyclic methylidene carbon atoms, is approximately 3 Å, which is much less than the 6.5 Å between STM features. Tunneling to different ends of the TCNQ molecule would require that the charge density within the TCNQ molecules in the tetramers be highly polarized, with the corresponding state density modulated along the stacks. The absence of intramolecular polarization in images of the (001) face, however, argues against this interpretation.

of tunneling to these underlying states is not well understood, we attribute the apparently enhanced tunneling to the submerged TCNQ stack to mediation by the dication stacks. It is plausible that the positive charge of the dication stacks screens the charge of the submerged TCNQ stack, resulting in an increase in the potential drop between the tip and this region and a corresponding increase in the tunneling current.

Electronic Structure. The electronic structure of 1 can be described on the basis of extended linear chains of $\rho = 0.5$ TCNQ sites (ρ = the average charge per site) with electronic band structures based on linear combinations of lowest unoccupied molecular orbitals (LUMOs) of TCNQ. Extended Hückel calculations indicate that the TCNQ LUMO consists largely of contributions from the exocyclic methylidene carbon atoms with lesser contributions from the nitrogen and ring carbon atoms.[24] Since the TCNQ LUMO is partially occupied in 1, the corresponding bands derived from these orbitals are likely to be those nearest E_F. The dications, however, are closed-shell species with an 18-electron configuration and therefore are not likely to possess states in the vicinity of E_F. This is supported by comparison of the electrochemical redox potentials of these two species ($E°_{TCNQ/TCNQ^-} = +0.19$ V vs SCE in acetonitrile, whereas the dication is not oxidized or reduced within the solvent limits of −2.0 to +2.0 V vs SCE). Interpretation of the STM images therefore is best described in terms of available states on the TCNQ stacks.

The semiconducting properties and crystal structure of 1 suggests that the *local* electronic structure plays an important role in the properties of 1. A tight-binding approximation based upon a linear combination of the TCNQ LUMOs in the tetramers therefore provides a valid description of the band structure associated with the extended TCNQ stacks. Each $(TCNQ)_4^{2-}$ tetramer comprises four TCNQ LUMOs whose linear combinations provide four new wavefunctions Ψ_1–Ψ_4 (Figure 7, left). If the spin pairing energy (U) is small compared to the Hückel overlap integral (β), Ψ_1 will be completely filled. Conversely, when $U > \beta$, significant population of Ψ_2 can result.

The tight-binding band approximation incorporates the localized states Ψ_1–Ψ_4 into extended states (Figure 7, right). When $U < 4t$ (t = the transfer integral, the tight-binding equivalent of β), a $\rho = 0.5$ system can adopt a metallic band structure in which the band is 1/4-filled. The lower portion of the band is predominantly bonding in character and the upper portion antibonding, reflecting the range of energy from Ψ_1 to Ψ_4. The dispersion of states arises from the various linear combinations of Ψ_1–Ψ_4. If the Coulomb repulsion energy (U) is large, a high-spin state can result (U is the tight-binding equivalent of the spin pairing energy described above). The energy of this state can be further lowered by formation of a magnetic $4k_F$ structure which results in dimerization of the one-dimensional stacks, lowering the electron kinetic energy, and formation of a bandgap. Further lattice distortion to a tetramerized stack and formation of a diamagnetic $2k_F$ structure can occur if the energetic cost of the lattice distortion can be compensated by the additional lowering of the electron kinetic energy or favorable changes in Coulombic terms. Comparison of the localized and tight-binding band descriptions of the $2k_F$ structure gives valence and conduction bands consisting of states based on Ψ_1 and Ψ_2 states, respectively. In this case, U is less than the energy gap between the valence and conduction bands. In contrast, the valence band of the $4k_F$ structure consists of states based on both Ψ_1 and Ψ_2. The upper band would comprise states based on Ψ_3 and Ψ_4, with the former dominating at the bottom of the band. The $4k_F$ structure is favored when U is large, synonymous with a large spin pairing energy in Ψ_1.

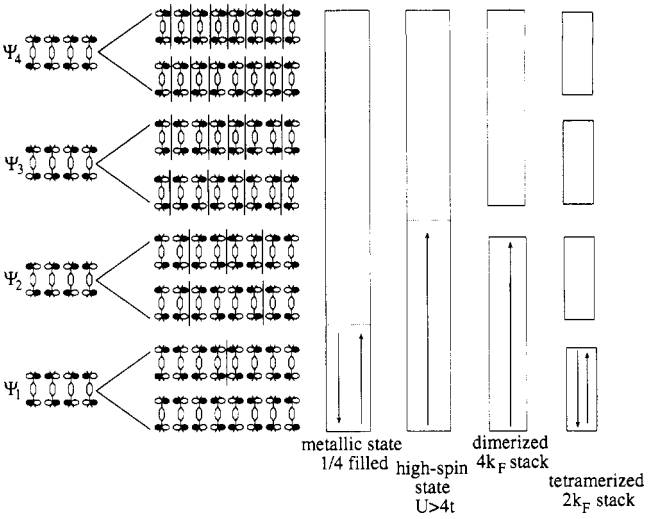

Figure 7. Schematic representation of the Ψ_1–Ψ_4 linear combinations of TCNQ LUMOs in the $(TCNQ)_4^{2-}$ tetramer (left), octameric segments of the linear combinations of Ψ_1–Ψ_4 (center), and bands according to the tight-binding approximation based on these combinations (right). The filled levels of the $2k_F$ and $4k_F$ states correspond to linear combinations of Ψ_1 and $(\Psi_1 + \Psi_2)$, respectively. The lowest and highest states of each band of the $2k_F$ structures are shown. For purposes of clarity only the dominant wave functions on the exocyclic methylidene carbon atoms are shown. Each TCNQ LUMO is partially filled ($\rho = 0.5$). The nodal planes, indicated by the solid lines, portray the patterns of nodes in the higher Ψ_2 states and lower Ψ_3 states that are believed to correspond to the tunneling current contrast at $a/2$.

The crystal structure, magnetic susceptibility and EPR studies of 1 indicate that at room temperature the electronic structure is dominated by the antiferromagnetic $2k_F$ structure which is equivalent to a filled Ψ_1 state in the local description. *This suggests that electron tunneling from the tip to 1 would primarily involve states in a conduction band based on* Ψ_2. The bottom of this band consists of in-phase linear combinations of Ψ_2. Magnetic susceptibility and EPR studies indicated, however, the presence of a high-spin triplet excitonic state corresponding to an approximately 5% contribution of the $4k_F$ structure ($\Psi_1 + \Psi_2$) states at room temperature. Participation of the $4k_F$ state is expected to affect the electron tunneling characteristics in that tunneling would involve higher Ψ_2 states, which correspond to out-of-phase linear combinations of Ψ_2. Alternatively, states in the lower portion of the Ψ_3 band derived from in-phase combinations of Ψ_3 may play a role if the $4k_F$ structure is present. The phase relationships of the linear combinations of the higher Ψ_2 states and the lower Ψ_3 states provide nodal planes at $a/2$, the node density increasing with increasing energy. Filling of the Ψ_2 states also corresponds to a shift of charge density towards the ends of the $(TCNQ)_4^{2-}$ tetramer at the expense of the center, in accord with the canonical description $(TCNQ)_2^-(TCNQ)_2^-$ assigned to the coupled electrons of the triplet species in our previous EPR studies. This canonical description implies dimerization of the TCNQ stacks as expected for the $4k_F$ structure.

Relationship between the LDOS, $2k_F$, and $4k_F$ Charge Density Waves. The tunneling current contrast periodicity of a on the (001) face is consistent with the phase relationships expected for tunneling into the lower

(24) (a) Berlinsky, A. J.; Carolan, J. F. *Solid State Commun.* **1974**, *15*, 795–801. (b) Lowe, J. P. *J. Am. Chem. Soc.* **1980**, *102*, 1262–1269.

portion of the conduction band of the $2k_F$ structure, which consists of states based on in-phase combinations of Ψ_2. The secondary alteration at $a/2$, however, suggests participation of states in the upper portion of the conduction band of the $2k_F$ structure, which consists of states based on out-of-phase combinations of Ψ_2. Alternatively, tunneling at $a/2$ intervals can be viewed as tunneling into the lower portion of the upper band in the $4k_F$ structure, which consists of states based on in-phase combinations of Ψ_3 (note that the in-phase linear combinations of Ψ_3 are identical to the out-of-phase combinations of Ψ_2). In either case, the increase in nodal density at $a/2$ relative to states derived from linear combinations of Ψ_1 or the lower portion of the Ψ_2 band is expected to give tunneling features tending toward those observed on the (001) face. Although the crystal structure of **1** strongly implicates the $2k_F$ tetramerized structure, these STM results clearly indicate the $4k_F$ contribution to the electronic structure of **1**. This is in agreement with our previous magnetic susceptibility and EPR measurements which established a roughly 5% contribution from the $4k_F$ structure at room temperature.

The absence of tunneling current corrugation at $a/2$ on the (010) face may indicate that images of this face reflect tunneling into states different than those involved in tunneling on the (010) face, for example, states with greater contribution from higher levels of Ψ_3 or possibly lower levels of Ψ_2 where nodal structure at $a/2$ is absent (Figure 7). However, the stacks imaged on the (010) face are crystallographically identical to those on the (001) face. Images of the (010) face were more difficult to obtain and generally were of poorer quality than the (001) face, which we attributed to the apparent lower conductivity of the (010) face. Accordingly, the absence of the $a/2$ alternation in images of the (010) face may be an artifact of this reduced conductivity.

The localization of state density evident from the tunneling current corrugation in the STM images can be described reasonably as charge density waves (CDWs), mixed waves of charge density modulation and periodic lattice distortion. Previous STM studies have noted CDWs on two-dimensional transition-metal chalcogenides such as TaS_2 and VSe_2.[14a,22] Since the periodicity of the tunneling current and the crystallographic lattice parameters are equivalent, the observed DOS represent a *commensurate* CDW.[25] These presence of commensurate CDWs can account for the semiconducting properties of **1**. Notably, there are *two* distinct one-dimensional CDWs in adjacent columns that are distinguished by different tunneling current contrast. The images obtained on the (001) and (010) faces are representations of the same pair of one-dimensional CDWs probed from near orthogonal directions. This CDW state is present in **1** at room temperature; due to thermal instability of **1** at high temperatures it is not possible to observe the actual CDW transition.

Particularly noteworthy is the *anti-phase modulation of tunneling current that is evident in the STM images of 1*. STM observations of anti-phase modulation has been noted previously for the transition-metal chalcogenide TaS_3, which has a high degree of one-dimensional character.[26] To our knowledge this is the first STM observation of CDWs, and the accompanying anti-phase modulation, on the surface of a molecular organic solid. The anti-phase modulation also is evident on the (010) face,

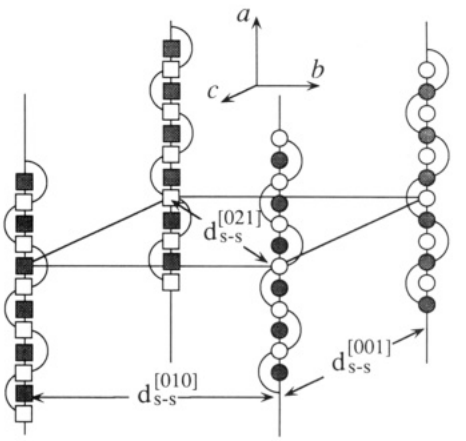

Figure 8. Schematic representation of the anti-phase modulation between TCNQ stacks. The unshaded and shaded regions denote the absence and presence of state density. The two crystallographically independent TCNQ stacks in **1** are represented by the columns of circles and squares.

although the modulation primarily conforms to intervals of a rather than $a/2$ as described above. Anti-phase modulation of one-dimensional CDWs has been noted for other low-dimensional organic solids based on diffuse X-ray scattering studies,[27] with three-dimensional ordering of CDWs experimentally observed below the Peierls transition temperature.[28]

The charge localization implicit in the CDWs can result from substantial interstack Coulomb repulsions *between* stacks which can be minimized by modulation of the charge density between stacks at intervals corresponding to the charge alternation. The observation of this modulation between the one-dimensional CDWs on both faces confirms that these images are representations of the same pairs of CDWs and also corroborates the assignment of one of the CDWs on the (010) face to the TCNQ stack beneath the surface plane. The CDWs can be described by $q_i = q_0 \cos \Phi_i$, where q_i is the amplitude of the CDW and Φ_i the phase angle of the ith CDW with respect to a reference. The Coulomb interaction energy between two stacks is given approximately by eq 1, in which $\epsilon_\perp$ is the perpen-

$$U_{s\text{-}s}^{[hkl]} = (4\epsilon_\perp)^{-1} q_0^2 [2\kappa_0(2k_F d_{s\text{-}s}^{[hkl]})] \cos(\Phi_i - \Phi_j) \qquad (1)$$

dicular static dielectric constant, $\kappa_0(x)$ the complete elliptic integral of the first kind,[29] and $d_{s\text{-}s}^{[hkl]}$ the distance between TCNQ stacks along the $[hkl]$ direction.[30] Therefore, adjacent CDWs that are 90° out of phase will represent the minimum Coulombic energy. This modulation is depicted schematically in Figure 8, where $d_{s\text{-}s}^{[010]}$ and $d_{s\text{-}s}^{[001]}$ represent the distance between the stacks along the b and c directions, respectively. The Coulomb energy will also be affected by interactions between stacks along the [021] and [0$\bar{2}$1] directions, although these will be less significant than those along the [010] direction.

(25) Lee, P. A.; Rice, T. M.; Anderson, P. W. *Solid State Commun.* **1974**, *14*, 703–708.

(26) (a) Slough, C. G.; Coleman, R. V. *Phys. Rev. B* **1989**, *40*, 8042. (b) Gammie, G.; Hubacek, J. S.; Skala, S. L.; Brockenbrough, R. T.; Tucker, J. R.; Lyding, J. W. *Phys. Rev. B* **1989**, *40*, 11965.

(27) (a) Torrance, J. B. *Phys. Rev. B* **1978**, *17*, 3099. (b) Kagoshima, S.; Ishiguro, T.; Schultz, T. D.; Tomkiewicz, Y. *Solid State Commun.* **1978**, *28*, 485. (c) Abrahams, E.; Solyom, J.; Woynarovich, F. *Phys. Rev. B* **1977**, *16*, 5238.

(28) (a) Kobayashi, H.; Kobayashi, A. *Extended Linear Chain Compounds*; Miller, J. S., Ed.; Plenum Press: New York, 1982; Vol. 2, p 275. (b) Friedel, J. *Electron-Phonon Interactions and Phase Transitions*; Riste, T., Ed.; Plenum Press: New York, **1977**; Vol. 29, pp 1–49. (c) Kagoshima, S. *Extended Linear Chain Compounds*; Miller, J. S., Ed.; Plenum Press: New York, **1982**; Vol. 2, p 311.

(29) $\kappa_0(x)$ is the complete elliptic integral of the first kind, which for $x \gg 1$, $2\kappa_0(x) \approx (p/2x)^{1/2}e^{-x}$. In this case $x = 2k_F d_{s\text{-}s}^{[hkl]}$.

(30) (a) Saub, K.; Barisic, S.; Friedel, *J. Phys. Lett.* **1976**, *56A*, 302–304. (b) Heeger, A. J. In *Chemistry and Physics of One-Dimensional Metals*; Keller, H. J., Ed.; Plenum Press: New York, 1977; pp 87–135.

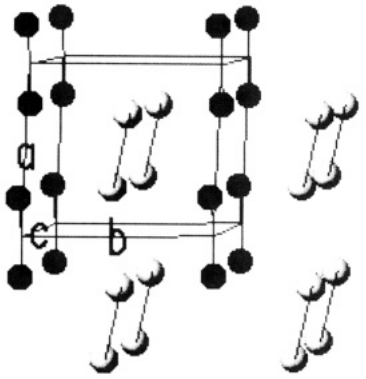

Figure 9. Position of the $(\eta\text{-}C_5Me_5)_2Ru(\eta^6,\eta^6\text{-}[2_2](1,4)\text{-cyclophane})^{2+}$ cations in 1 as viewed slightly off the [001] direction. The organic ligands have been omitted for clarity, with Ru^+ cation centers of the same molecule connected. The crystallographically unique molecules are indicated by different shading.

On the basis of the crystal structure, we expect that $U_{s\text{-}s}^{[010]} > U_{s\text{-}s}^{[001]} > U_{s\text{-}s}^{[0\bar{2}1]} > U_{s\text{-}s}^{[\bar{0}21]}$ because $d_{s\text{-}s}^{[010]}$ (on the *ab* face) represents the smallest interstack contact. Coulomb interactions between stacks along the other directions will be smaller owing to larger values of $d_{s\text{-}s}$. For example, the interactions between stacks in the (010) plane are smaller because of larger $d_{s\text{-}s}$ ($d_{s\text{-}s}^{[001]} = c$) and the presence of interleaving dication stacks that are expected to have a relatively large value of $\epsilon_\perp$. This is evident from the STM images: adjacent stacks on the (001) plane are anti-phase modulated along the [010] direction, whereas the stacks on the surface of the (010) face separated by the dications are in phase along the [001] direction.

The observation of anti-phase modulated CDWs strongly suggest that Coulomb interactions between one-dimensional chains[30a] play an important role in the crystal and electronic structure of 1 rather than simply a lowering of the electron kinetic energy. On a molecular level, the anti-phase tunneling current modulation at $a/2$ on the (001) face can be attributed to contributions from the canonical form $(TCNQ)_2^-(TCNQ)_2^-$ of the $4k_F$ structure. The charge is localized on the $(TCNQ)_2^-$ dimers in an anti-phase manner so as to reduce charge repulsion between the stacks. The proximity of the stacks and the ability to minimize the Madelung energy by anti-phase amplitude modulation lowers the energetic cost associated with the lattice distortion from the unobserved metallic state with uniform TCNQ stacks. The onset of 3-D CDWs in other organic conductors resulting from interstack Coulomb interactions such as those observed in 1 has been reported to occur below the temperature at which 1-D CDWs are formed.[31] The lower temperature for the 3-D CDW onset has been attributed to shorter correlation lengths in the transverse direction owing to reduction of the interstack Coulomb interaction by counterions. In the case of 1, however, interactions between the TCNQ stacks along the [010] direction are not mediated by cations, and strong Coulomb correlations can be expected. *Significantly, the two crystallographically independent dications are also anti-phase modulated with respect to adjacent stacks* (Figure 9). Although the actual charge distribution in the dications is not known, the centroids of the $(\eta\text{-}C_5Me_5)_2Ru(\eta^6,\eta^6\text{-}[2_2](1,4)\text{cyclophane})^{2+}$ dications are anti-phase modulated along [001] at intervals of $a/2$. This strongly suggests that Coulombic *attractive* forces between the localized charges of the CDW and the dication also contribute to the observed electronic structure. That is, the dications likely play an important role in pinning the CDW in a commensurate manner.

The crystal structure of 1 therefore is a manifestation of several energetic terms, including van der Waals forces associated with close packing, π–π overlap between TCNQ molecules in each stack, electronic interactions between stacks (albeit negligible) and Coulombic interactions associated with the ionic charges. The Coulombic interactions induce charge localizations, thereby stabilizing the magnetic $4k_F$ $(TCNQ)_2^-(TCNQ)_2^-$ state that is manifested as EPR-observable triplet excitons. The formation of triplet excitons would not be possible if $U < 4t$ and the ground state of 1 was metallic. The anti-phase modulation and the accompanying reduction in total free energy therefore facilitates formation of the high-spin triplet state by condensation of charge on the $(TCNQ)_2^-$ dimers.

The STM images of the (001) face provide some indication of the differences in the electronic properties of the two crystallographically unique TCNQ stacks. The crystal structure indicates that stack B has more uniform interplanar spacing (i.e., larger bandwidth) than stack A but a smaller topographical corrugation along the stacking axis (Figure 2). Notably, the apparent height corrugation is greater in the column denoted A in Figure 4. This column also exhibits less continuity of tunneling current along the stacking axis compared to column B. These observations support the assignment of two crystallographically unique TCNQ stacks to their corresponding columns of tunneling current as denoted in Figure 4. It should be noted, however, that for one-dimensional semiconductors with CDWs in which the Fermi surface has collapsed to a single point, the STM data may not have a *direct* relationship to the position of the atoms in the unit cell.[32] That is, the electronic contribution to $\rho(r,E_F)$ may dominate over the tip–sample distance effects, as indicated above. Accordingly, the assignments of the tunneling current to specific TCNQ stacks should be viewed with caution.

Nevertheless, the larger bandwidth suggested by the more significant tunneling continuity in column B is consistent with the more uniform spacing in stack B. This larger bandwidth may suggest that column B is responsible for the $4k_F$ magnetic state, but the STM studies do not allow a definitive assignment of the triplet species. The intervals of tunneling current amplitude ($a/2 = 6.9$ Å) are similar to the 7.5-Å value determined by EPR for the average separation between coupled electrons. We note that the STM data also suggest a 7.8-Å separation between tunneling current maxima on adjacent stacks. This may suggest that the coupled electrons of the triplet exciton may be located on adjacent stacks. Although very weak interchain coupling between spins (<0.001 eV) has been suggested for the triplet excitons of $MEM(TCNQ)_2$[33] (MEM = *N*-methyl-*N*-ethylmorpholinium), this is not likely in 1 given the large spin exchange coupling (0.08 eV) and our previous single-crystal EPR studies of 1[8] that indicated that the major triplet species was coincident with the TCNQ stacking axes.

Conclusions

The results described above clearly show that STM can provide highly resolved images of the crystal planes of

(31) (a) Comes, R.; Lambert, M.; Launois, H.; Zeller, H. R. *Phys. Rev. Lett.* **1971**, *27*, 1060. (b) Renker, R.; Pintshovius, L.; Glaser, W.; Rietschel, H.; Come, R.; Liebert, L.; Drexel, W. *Phys. Rev. Lett.* **1974**, *32*, 836. (c) Comes, R.; Lambert, M.; Zeller, H. R. *Phys. Status Solidi B* **1973**, *58*, 587. (d) Lynn, J. W.; Iizumi, M.; Shirane, G.; Werner, S. A.; Saillant, R. B. *Phys. Rev. B* **1975**, *12*, 1154.

(32) Tersoff, J. *Phys. Rev. Lett.* **1986**, *57*, 440.
(33) Oostra, S.; De Lange, P.; Visser, R. J. J. *J. Phys. C* **1983**, *44*, 1383.

molecular organic conductors which can be correlated with the electronic structure and molecular topology of crystal faces. Significant tunneling current is observed on two different crystal planes of **1** that can be assigned to tunneling into the conduction band of commensurate CDW structures based on contributions from the $4k_F$ excited state in addition to the $2k_F$ ground state. The STM data therefore clearly show the charge localization responsible for the semiconducting properties of this material and the mobile triplet excitons observed in its EPR spectrum. Tunneling current between the one-dimensional CDWs is negligible, reflecting a lack of state density between TCNQ anion stacks that is consistent with the low-dimensional nature and semiconducting properties of **1**. The observed anti-phase modulation of the CDWs results from strong Coulomb repulsion between two crystallographically unique TCNQ anion stacks and Coulomb attraction between the TCNQ anion stacks and the $(\eta\text{-}C_5Me_5)_2Ru(\eta^6,\eta^6\text{-}[2_2](1,4)\text{cyclophane})^{2+}$ cations. Unfortunately, attempts to obtain more detailed information about the CDW state by current voltage curves have not been successful. The data obtained are generally very noisy and not reproducible; we presume that the low conductivity of this material is responsible for this behavior.

These studies demonstrate that STM can play an important role in the characterization of low-dimensional solids, providing insight into their electronic structure. We also anticipate that the detailed characterization of the surface topography and electronic structure provided by the STM will advance understanding of electrochemical crystal growth mechanisms. The factors that control the morphology of electrochemically grown crystals, which typically tend to grow as anisotropic needles with a clearly defined preference for growth along the stacking axis, are of particular interest. The morphology of crystals depends upon the relative rates of growth along different directions, which in turn will depend upon the electron-transfer rate, the rate of attachment of molecules or their aggregates to the different crystal faces, and adsorption of solvent or impurity molecules. The observation of tunneling current on the both the (001) and (010) planes indicates that electron transfer to TCNQ molecules at these faces is feasible and can account for the crystal growth on both faces. Characterization of these surfaces on the molecular level as provided by STM also may provide a basis for nanoscale STM assisted synthesis on single crystals of these materials.

Acknowledgment. The support of the National Science Foundation (NSF/DMR-9107179), the Office of Naval Research, and the NSF Center for Interfacial Engineering (NSF Engineering Research Centers Program, CDR 8721551) is gratefully acknowledged.

Registry No. 1, 142981-53-1.